JACS
JOURNAL OF THE AMERICAN CHEMICAL SOCIETY
Article
pubs.acs.org/JACS

Single Enzyme Experiments Reveal a Long-Lifetime Proton Leak State in a Heme-Copper Oxidase

Mengqiu Li,[†] Sune K. Jørgensen,[‡] Duncan G. G. McMillan,[†] Łukasz Krzemiński,[†] Nikolaos N. Daskalakis,[†] Riitta H. Partanen,[†] Marijonas Tutkus,[‡] Roman Tuma,[§] Dimitrios Stamou,*[,‡] Nikos S. Hatzakis,*[,‡] and Lars J. C. Jeuken*[,†]

[†]School of Biomedical Sciences, University of Leeds, LS2 9JT Leeds, U.K.

[‡]Department of Chemistry, Nano-Science Center and Lundbeck Foundation Center for Biomembranes in Nanomedicine, University of Copenhagen, 2100 Copenhagen, Denmark

[§]School of Molecular and Cellular Biology, University of Leeds, LS2 9JT Leeds, U.K.

Supporting Information

ABSTRACT: Heme-copper oxidases (HCOs) are key enzymes in prokaryotes and eukaryotes for energy production during aerobic respiration. They catalyze the reduction of the terminal electron acceptor, oxygen, and utilize the Gibbs free energy to transport protons across a membrane to generate a proton (ΔpH) and electrochemical gradient termed proton motive force (PMF), which provides the driving force for the adenosine triphosphate (ATP) synthesis. Excessive PMF is known to limit the turnover of HCOs, but the molecular mechanism of this regulatory feedback remains relatively unexplored. Here we present a single-enzyme study that reveals that cytochrome bo_3 from *Escherichia coli*, an HCO closely homologous to Complex IV in human mitochondria, can enter a rare, long-lifetime leak state during which proton flow is reversed. The probability of entering the leak state is increased at higher ΔpH. By rapidly dissipating the PMF, we propose that this leak state may enable cytochrome bo_3, and possibly other HCOs, to maintain a suitable ΔpH under extreme redox conditions.

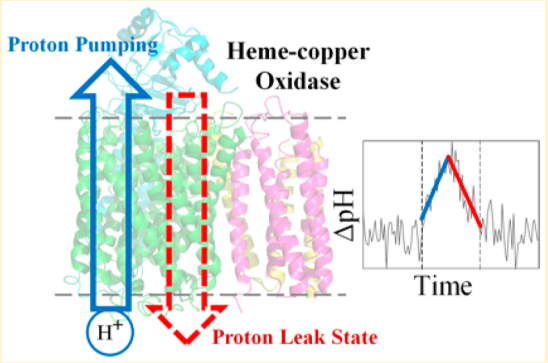

INTRODUCTION

One of the main roles of oxidative phosphorylation in mitochondria and bacteria is maintaining a proton-motive force (PMF) across the inner or plasma membrane, thereby providing most of the energy for the synthesis of adenosine triphosphate (ATP) in aerobic environments. The PMF is formed by transferring or pumping protons across the lipid membrane, generating a transmembrane electrochemical potential and transmembrane pH difference (ΔpH). During aerobic respiration, electron-transport chains of oxidative phosphorylation terminate with heme-copper oxygen reductases (HCOs), in which a heme-copper binuclear center (BNC) binds and reduces dioxygen to water. The HCO in mitochondria is a cytochrome *c* oxidase known as Complex IV. Complex IV and a bacterial homologue, cytochrome bo_3 from *Escherichia coli*, belong to the A1 subgroup of Type-A HCOs, which typically pump one proton per electron, therefore four protons per dioxygen molecule.[1] The reduction of dioxygen is further coupled to the uptake/release of four charges (protons and/or electrons), adding up to a total of eight charges transported across the membrane for each dioxygen that is reduced. Type-A HCOs possess two conserved proton channels, known as the K- and D-channel, both leading to the BNC.[2−5] The K-channel facilitates the transportation of "chemical protons" that react with dioxygen to form water; the D-channel facilitates both the uptake of "chemical protons" and the transportation of all the pumped protons.[6−9] Both channels take up protons from the same side of the membrane: the matrix side in mitochondria or the cytoplasmic side in bacteria.[2,3]

Despite various high-resolution structures[2−4] and extensive biochemical and biophysical research,[6−15] a distinct understanding of the molecular mechanism by which oxygen reduction is coupled to proton pumping is still elusive, while the manner by which turnover is controlled by the PMF remains relatively unexplored. HCOs, including cytochrome bo_3, have been observed to reduce activity in the presence of high PMF.[16,17] A "slip" in their pumping stoichiometry (decrease in the proton-to-electron ratio) has been observed in many HCO studies[16] and also for other transport systems.[18] The implications of these alterations in stoichiometry have been previously discussed for HCOs and for pumping ATPases and transporters in healthy and disease states.[5,18−21] Slips in

Received: August 19, 2015
Published: November 30, 2015

DOI: 10.1021/jacs.5b08798
J. Am. Chem. Soc. 2015, 137, 16055−16063

substrate transport have been proposed to act as a "safety valve" through which excess driving force can be dissipated[18] and it is proposed to be a mechanism by which HCOs can optimize the condition for ATP synthesis.[16] Maintaining such balance is important since high PMF and a highly reduced electron-transport chain (high ratios in ubiquinol/ubiquinone and $NADH/NAD^+$) have been linked to increased production of reactive oxygen species (ROS) in mitochondria,[16,22] which has been implicated in aging, cancer, and other diseases.[23,24]

Current understanding of the pumping mechanism of HCOs primarily relies on ensemble studies averaging the behavior of multiple pumps.[25−28] While providing a great wealth of information, these studies average out rare events during continuous turnover, masking the dynamic heterogeneity of HCOs and effectively preventing detection of leak states. Single-molecule studies on the other hand offer the exquisite ability to directly observe the temporal fluctuations of individual enzymes and their role in regulation of their activities.[29,30] Single-enzyme studies were pioneered for ion channel current recordings and, more recently, single-enzyme studies on transporters have visualized the structural dynamics of transmembrane helices.[31] However, neither method can directly report on proton pumping during continuous turnover. Here, we have developed a novel platform that can directly observe the proton transfer of single cytochrome bo_3 enzymes for prolonged periods (up to 100 s; Figure 1a). Our studies

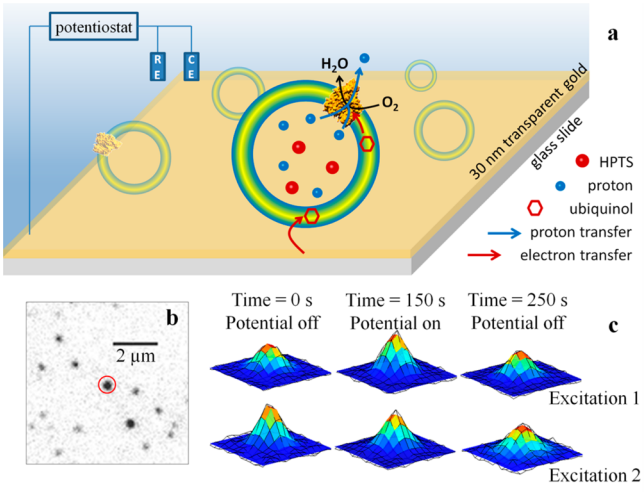

Figure 1. Schematic diagram of the experimental method. Proton uptake/release activity of reconstituted cytochrome bo_3 is controlled by reducing ubiquinone electrochemically (a). The change in intravesicular pH is determined via an encapsulated pH-sensitive fluorescent dye, 8-Hydroxypyrene-1,3,6-trisulfonic acid (HPTS) (a). A color-inverted fluorescent image (b) and the fitting of the fluorescence of the circled proteoliposome by a Gaussian function (c) (the grid is raw data, and the colored surface is the fitting result) are shown. The sample image in (b) shows a small area of the whole image which typically contains hundreds of (proteo)liposomes.

reveal that cytochrome bo_3, a representative HCO enters a rare, long-lifetime "leak state" during which protons rapidly leak or are transported back along the transmembrane electrochemical potential and ΔpH. Our findings support a view in which one of the underlying causes of the previously observed reductions in the H^+/e^- stoichiometry is a leak state, which provides new insights into the molecular mechanism of proton pumping in HCOs and its regulation by excessive ΔpH. The novel method described in this study also adds to the ever expanding library of techniques to study single molecules on surfaces by combining optical and electrochemical methods.[32]

RESULTS AND DISCUSSION

This study was carried out on cytochrome bo_3, an ubiquinol oxidase from *E. coli*. A key difference between bo_3 and cytochrome *c* oxidases such as Complex IV is their electron donor, which are ubiquinol and cytochrome *c*, respectively. This allowed us to design a combined electrochemical-microscopic experimental setup for single-enzyme analysis as schematically shown in Figure 1. In this setup, which is described in detail in the Materials and Methods, proteoliposomes containing cytochrome bo_3 are sparsely adsorbed on a transparent ultrasmooth thin gold electrode within an electrochemical cell. The gold is modified with a self-assembled monolayer of 6-mercapto-hexanol, which renders it hydrophilic and allows immobilization of the proteoliposomes, that retain the pH sensitive fluorophore. To approach single-enzyme conditions, the proteoliposomes are made using a very low protein-to-lipid ratio. Because of the low protein-to-lipid ratio, most of the liposomes in the experiments do not contain a protein and we will adopt the term "(proteo)liposomes" in the remainder of this text to reflect this. Image analyses procedures are used to exclude (proteo)liposomes that are close together by picking circular and separated bright spots with a typical size that is consistent with single vesicles (see Materials and Methods). Nonetheless, this analysis will not be able to detect if two (proteo)liposomes are less than 200 nm apart. As described in the Supporting Information, simulations based on assumption that vesicles randomly adsorb on the surface suggest that this will occur in only 0.3 ± 0.2% of fluorescent spots. Because most (proteo)liposomes do not contain an enzyme, the probability that two proteoliposomes with an enzyme coincide in a single fluorescent spot is much lower.

The (proteo)liposomes also contain ubiquinone that is electrochemically reduced to ubiquinol, thereby activating the oxygen reducing activity of cytochrome bo_3. The (proteo)-liposomes are loaded with a pH-sensitive fluorescent dye (hydroxypyrene-1, 3, 6-trisulfonic acid trisodium salt (HPTS)) and the electrochemical cell is placed in an epi-fluorescent microscope that monitors the fluorescence which, with the use of separately determined calibration data and the measured vesicle sizes, is converted to intravesicular pH and the number of transported protons in individual (proteo)liposomes (see Supporting Information for the calibration procedure).

Figure 2 shows a collection of typical (proteo)liposome time traces, where the intravesicular pH changes (see Figure S1) are used to calculate the cumulative number of transported protons. Because of the low protein-to-lipid ratio used, the majority of the observed (proteo)liposomes were plain liposomes and did not portray any change in pH upon reducing the ubiquinone pool electrochemically (Figure 2f). During the time window the ubiquinone pool was electrochemically reduced (dashed lines in Figure 2), about 15% of the observed (proteo)liposomes displayed significant pH changes ($0.1 < \Delta pH < 1$ and in rare cases up to about 2 units). Indeed, the average number of cytochrome bo_3 complexes per (proteo)liposome is calculated to be 0.16 using the average protein-to-lipid ratio and the average (proteo)liposome size (see Materials and Methods for details). Assuming Poissonian dilution of proteins/liposome we would then expect 15% of liposomes to contain one active protein and ∼1% of liposomes

DOI: 10.1021/jacs.5b08798
J. Am. Chem. Soc. 2015, 137, 16055−16063

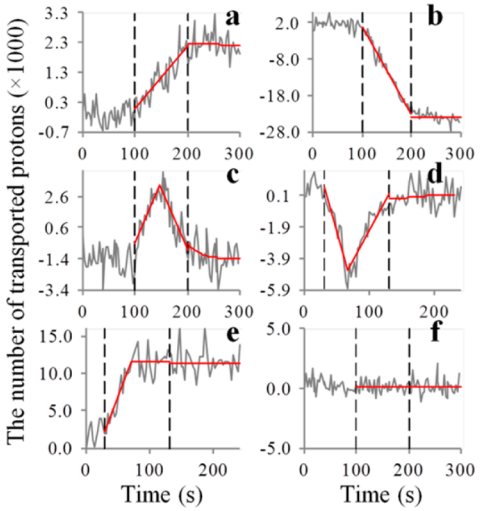

Figure 2. Examples of time traces of (proteo)liposomes. Example traces are given for proteoliposomes where protons are pumped throughout the application of the electrochemical potential (a,b), proton leakage (c,d), proton uptake/release cessation without leakage (e). An example trace of a liposome without cytochrome bo_3 is also shown (f). Red lines in the example traces (a–f) are fits to the data (gray) as explained in the text. Proton uptake/release activity was initiated by applying an electrochemical potential between time points indicated by the vertical dashed lines.

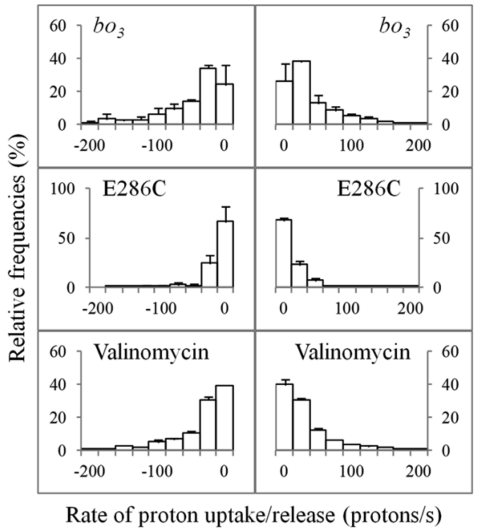

Figure 3. Distribution of proton translocation rates for (top) wild-type cytochrome bo_3 (middle) E286C cytochrome bo_3 and (bottom) wild-type cytochrome bo_3 in the presence of valinomycin. Cytochrome bo_3 was orientated both ways in the single-enzyme proteoliposomes and relative frequencies are separated for "proton uptake" (positive rates) and "proton release" (negative rates). The rates are determined from the slope of the analyzed data for which examples are shown in Figure 2. The error bars represent the standard error of the mean.

to have more than one protein. This calculation is concurrent with our hypothesis that most (proteo)liposomes displaying pH changes are due to proton uptake/release by single enzymes, which however could not be confirmed via direct experimental measurement. Deviations from the calculated average number or proteins/liposome are expected because of the polydispersity in (proteo)liposome diameter (71 nm with a full width at half maximum (fwhm) of 45 nm, Figure S8) and hence surface area. Additional deviations at the level of single particles could be present due to the heterogeneous distribution of proteins[33] and/or lipids.[34]

The pH values were observed to both increase and decrease (Figure 2a and 2b, respectively; hereafter these proteoliposomes will be described as "active" liposomes or vesicles), indicating cytochrome bo_3 was present in both orientations in the proteoliposomes. About 76% of active vesicles show a pH increase consistent with a "right-side out" orientation. The single-enzyme traces reveal a distribution in turnover rates (Figure 3), while in more than 10% of cases, cytochrome bo_3 was observed to abruptly halt proton uptake/release (Figure 2e). Such dynamic heterogeneity and "stalling" of activity was observed for enzymes in both orientations and is a feature typically observed for (single) enzymes.[29] Importantly, however, a significant fraction of our single enzyme traces (7.2 ± 1.5%) also show abrupt turns in pH changes, rapidly destroying formed ΔpH even when the potential was still applied to reduce the ubiquinone pool. Such events were observed for cytochrome bo_3 in both orientations, as shown in Figure 2c and d.

In order to quantitatively analyze the heterogeneous activity of the enzyme and resolve the distinct phases in the time traces (e.g., Figure 2c–e) without human bias, an automatic trace analysis was coded and its results are visualized by the red lines in Figure 2 (see Materials and Methods for details). To reproduce the findings, they were recorded in two separate laboratories, first in Copenhagen and then in Leeds. Two different methods varying in experimental setup, pH-dependent fluorescent probe (HPTS vs SNARF-1), and materials were used, which further support their validity (see the Independent Verification section in the Supporting Information). Two different image and data analysis procedures were also tested and compared, and both methods confirmed the conclusions presented below. The data analysis procedure resolves phases/events which are statistically distinctive (proton translocation, proton leakage and the stalling phase) within the time-traces and yields measurements such as the average proton translocation rate for each event, the duration of the event, and the ΔpH at the onset of each event.

The proton translocation rates correspond to an ensemble average of 73 ± 2.2 protons s^{-1} (Figure 3), which is less than the published activity of 520 electrons s^{-1} in reference[35] and 850 electrons s^{-1} in reference.[17] We ascribe this difference to various reasons: (a) only about half of the maximum activity of cytochrome bo_3 is reached at the electrochemical potential used to activate cytochrome bo_3 in the single-enzyme experiments (−0.2 V vs standard hydrogen electrode (SHE), Figure 4) and (b) V_{max} condition cannot be reached using ubiquinol-10 as the electron donor. Ubiquinol-10 is nearly identical to the native electron donor in *E. coli* (ubiquinol-8). However, previously reported values were measured using substrate analogues (decyl-ubiquinol[35] or ubiquinol-1[17]) under saturation conditions, while here ubiquinol-10 was added to the (proteo)-liposomes under nonsaturating conditions (1% w/w ubiquinol-10/lipid). Saturation of ubiquinol-10 in the membrane is not possible due a disrupting effect of high ubiquinol-10 concentrations and a previously reported substrate inhibition effect.[36]

Analysis shows that 7.2 ± 1.5% of the proton-transporting proteoliposomes abruptly switch to seemingly passive leaking within the potential window. The reproducibility and statistical robustness of our analysis is verified by 4 independent series of experiments with cytochrome bo_3 from two different over-

DOI: 10.1021/jacs.5b08798
J. Am. Chem. Soc. 2015, 137, 16055–16063

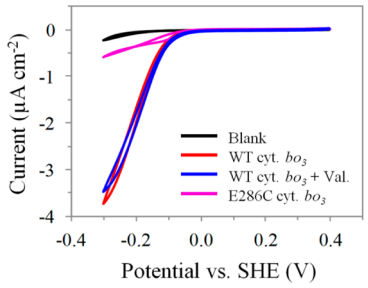

Figure 4. Cyclic voltammograms (CVs) of absorbed proteoliposomes of WT and E286C cytochrome bo_3. Electrode preparation and modification are identical to the single-enzyme experiments except that 150 nm gold was used, proteoliposomes were reconstituted with a higher protein-to-lipid ratio (1% w/w) and full layer of proteoliposomes were immobilized on the electrodes by incubating the electrode with 0.5 mg/mL proteoliposomes for 30 min. CVs (2 mV/s) were measured under ambient, aerobic conditions at 20 °C. The onset of ubiquinol-10 reduction in the proteoliposomes starts at about −0.05 V vs SHE. CVs of proteoliposomes before and after addition of 10 μM valinomycin are shown. A CV of the electrode surface prior to immobilization of proteoliposomes (blank) is also depicted.

expressing strains, which show maximum and minimum leak probabilities ranging from 2.9 to 9.5%. Statistically, these leak events are inconsistent with multiple enzymes per active vesicle, as it would require two oppositely orientated cytochrome bo_3 complexes to behave in certain patterns, e.g., one enzyme stopping and the other starting at about the same time or the slower enzyme halting activity first. To confirm that leak events are obtained from proteoliposomes containing single enzymes, the experiments were repeated with an average protein-to-lipid ratio 1 order of magnitude lower, where the stochastic probability of having two oppositely oriented protein complexes is 2 orders of magnitude lower (<0.1%). As expected, the number of (proteo)liposomes displaying pH changes was significantly reduced (2.5% ± 0.33%), but the abrupt switch was still observed for 3.2% ± 0.65% of the active vesicles (4 independent experiments with leak state percentages between 1.9 and 4.5%). We propose that these data further confirm that the leak activity is due to single proteoliposomes with single enzymes.

Although it is known that membrane pores can randomly form in the presence of ΔpH, pores are transient, submillisecond events.[37,38] The observed lifetime of the leaking events (>10 s) is thus inconsistent with spontaneous pore formation in the lipid membrane of the vesicles. Furthermore, the proton permeability of the reconstituted proteoliposomes was independently measured by applying a ΔpH to the reconstituted proteoliposomes and empty liposomes under nonturnover conditions. In both cases the recorded "background" proton leaking rate is significantly lower than the observed leak states of cytochrome bo_3 (Figure S2), confirming that background proton permeability is negligible under our conditions. Furthermore, the fact that we observe similar background proton permeability for proteoliposomes reconstituted with cytochrome bo_3 and empty liposomes verifies that leaking is not an artifact of the reconstitution method. Taken together the abrupt changes in proton transport direction are most likely due to single enzyme-related proton leakage into or out of the proteoliposomes.

A simple explanation for the observed leak events and stalling is that they are due to irreversible inactivation or damage to cytochrome bo_3. Because less than 10% of the proteoliposomes enter the leak state and because the time-span of the experiments is limited (up to 100 s of active turnover) it is not possible to directly observe the rare recovery events. In addition, there is also the possibility, albeit low, of proteoliposomes containing two enzymes (or two proteoliposomes are less than 200 nm apart) and thus registering "false" recovery events. We therefore analyzed the relative number of proteoliposomes in consecutive movies on the same electrode (Figure S3). The percentage of the proteoliposomes containing cytochrome bo_3 that actively take up/release protons does not decrease when movies were taken sequentially. The movies were taken from different areas on the same electrode, but lipid vesicles that were not being fluorescently imaged are still subjected to the same electrical potential applied to the gold electrode which would start the enzyme turnover. Therefore, if cytochrome bo_3 could not revert back to normal proton translocation after entering the leak state or the stalling phase, the percentage of active vesicles would have shown a continuous decline. The lack of such downward trend indicates that both the leak state and the stalling phase are reversible.

It is generally accepted that back-flow of protons during turnover of HCOs is prevented by a gate in the D-channel.[28,39] We hypothesized that the long-lived leak events are caused by a conformational change causing the gate to "open" allowing protons to freely flow back. Glutamic acid 286 (E242 in bovine heart Complex IV) is highly conserved in Type A1 HCOs and lies at the end of the D-channel.[1] It has been suggested that E286 is an integral part of the gating mechanism[28,39] and to test this hypothesis, the same measurement and analysis was applied using an E286C mutant.

In E286C cytochrome bo_3, proton translocation through the D-channel is blocked and protons are prevented from being pumped across the membrane.[39] It is worth noting that besides the pumped protons, redox reactions in cytochrome bo_3 result in a further net translocation of four "chemical protons" across the membrane: the reduction of every dioxygen molecule draws four protons from the cytoplasmic side and another four protons are released into the periplasm after the oxidation of two ubiquinols.[2] The E286C mutant is catalytically active (Figure 3 and 4) and thus able to generate a ΔpH via the net translocation of "chemical protons". We note here that ubiquinone is also protonated when electrochemically reduced at the electrode. However, since electrons cannot transfer across the lipid bilayer, this process takes up protons from solution only (i.e., from outside the vesicles) and should therefore not influence the intravesicular pH.

The orientation of E286C cytochrome bo_3 is similar to wild type (WT): 66% of proteoliposomes with E286C cytochrome bo_3 take up protons from the inside of the lipid vesicle (alkalinization), compared to 76% of WT. The oxygen-reducing activity of E286C cytochrome bo_3 as measured by the electrochemical current (Figure 4) is about 15−20% of that of wild-type cytochrome bo_3, depending on the potential at which the comparison is made. The lower proton-transporting activity of E286C cytochrome (22% of that of WT, Figure 3) is consistent with the lower oxygen reducing activity, although higher than expected considering the fact that E286C cytochrome bo_3 can only release/uptake one proton per electron rather than two for wild-type cytochrome bo_3. This we attribute to the data analysis and noise levels, as very low proton uptake/release rates are hard to detect.

The single-enzyme experiments show that the relative frequency by which E286C enters the leak state is significantly

DOI: 10.1021/jacs.5b08798
J. Am. Chem. Soc. 2015, 137, 16055−16063

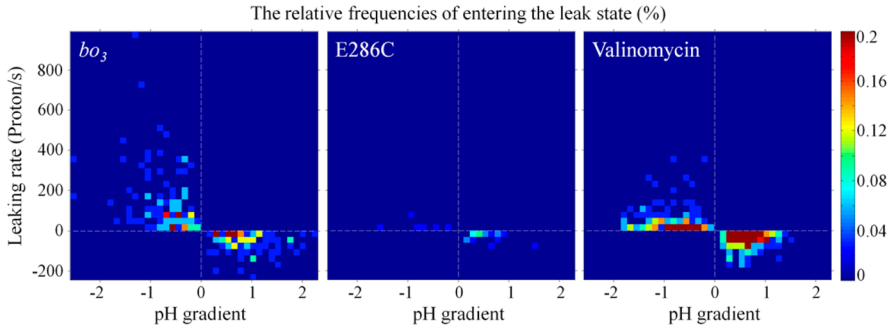

Figure 5. The relative frequency (in percentage) of entering the leak state during turnover in relation to the leaking rate and the ΔpH formed prior to the start of the leaking events. These figures are two-dimensional histograms generated in the same way as the conventional one-dimensional histogram (the color of the pixels is equivalent to the height of the bars in histogram bar chart). The sum of the relative frequency values in each heat map equals to the total relative frequency of proteoliposomes entering the leak state in the corresponding experiment. The ΔpH is the intravesicular pH minus the pH of the bulk solution (set constant at 7.4).

reduced to 0.6% (0.5% and 1% in two independent data sets each containing eight and 20 movies, respectively), compared to 7.2% for wild-type cytochrome bo_3. Besides the significantly reduced percentage of leak events observed for E286C cytochrome bo_3, the leaking rates are also significantly lower for E286C (25.5 ± 4.1 H^+/s vs 102.3 ± 11.2 H^+/s for the wild-type, Figure 5). We propose that these results further substantiate that the leak events observed from wild-type cytochrome bo_3 are caused by a leak state of the proton pump and not by oppositely orientated enzymes or pore formation in the lipid membrane. Although the results from the E286C mutant confirm that protons leak through the protein, they do not unambiguously show that protons flow via the D-pathway and more work is needed to identify the leak pathway. Because this mutant is less active than WT, the E286C mutation could allosterically reduce the probability that a leak state is formed. Indeed, on average, the lifetime of proton uptake/release in E286C cytochrome is about 25% longer than WT (Figure S4), but as lifetimes longer than 100s were capped because of the technical limitations on for how long an experiment can continue, this should be considered a lower limit. Therefore, there is an indication that the E286C mutant may have a longer lifetime for proton uptake/release. Related to this, the "stalling" behavior was observed in only 4% of the active vesicles.

We next examined whether the existence of the leak state may have a potential regulatory role. A possible cause that triggers cytochrome bo_3 into the leak state is a thermodynamically limiting PMF, i.e., high ΔpH and/or high membrane potential. Figure 5 shows that the leak states may be initiated at all ΔpH (horizontal axis in the heat map), and many leaking events started at low ΔpH. However, the relative frequency shown in Figure 5 is the frequency observed for the total population of active vesicles, which does not take into account that the majority of active vesicles never reached a high ΔpH or the fact that high ΔpH are only obtained for a relatively short time periods (Figure 6a). Figure 6d shows that by normalizing the frequency of the leak state against the relative occurrence of a ΔpH, the leak states is more likely to be initiated at higher ΔpH. The result of Kendall tau rank correlation test shows that the relative frequency of entering a leak state from all repeated experiments is indeed positively correlated to the ΔpH ($p < 0.01$, $\tau = 1$). The same analysis shows that the probability of entering a stalling phase is similarly correlated to the ΔpH (Figure 6e). Thus, our data suggest that cytochrome bo_3 might have evolved two mechanisms to control excessive ΔpH and

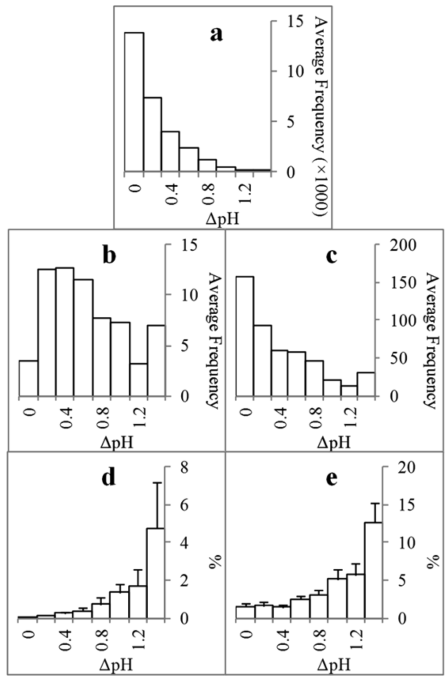

Figure 6. The relative frequency (in percentage) of cytochrome bo_3 entering the leak state or stalling phase within the time resolution of the experiment as a function of ΔpH. (a) the average frequencies that a ΔpH is encountered during a 2.6 s period of the time trace (i.e., the time resolution); (b,c) the distribution of the ΔpH formed just before entering the leak state or stalling phase, respectively; (d,e): the relative frequency of cytochrome bo_3 entering the leak state or stalling phase, respectively, as a function of ΔpH, which was calculated by dividing the frequencies in (b) and (c) by those in (a) for each independent experiment; the error bars show the standard error of the mean from 4 independent experiments. The negative ΔpH and negative proton release rates (acidification) have been converted to the absolute (positive) values. The ΔpH is the intravesicular pH minus the pH of the bulk solution (constant at 7.4).

either halts proton translocation or enters a proton leak state, dissipating the formed PMF. As mentioned above, the E286C mutant exhibits a longer lifetime of proton translocation. As the relative frequencies of the leak and stalling states of cytochrome bo_3 are dependent on the ΔpH (Figure 6), the longer lifetime could thus indirectly be due to the slower proton uptake/release activity of E286C cytochrome bo_3 compared to WT.

DOI: 10.1021/jacs.5b08798
J. Am. Chem. Soc. 2015, 137, 16055−16063

We next examined the role of transmembrane potential on triggering the leak state. Proteoliposomes are ideally suited for this as it has long been recognized that due to small volume in proteoliposomes, proton transport alone can build up a membrane potential.[40] To probe the influence of the membrane potential, the same experiment and analysis were performed on the wild-type cytochrome bo_3 in the presence of a potassium ion carrier, valinomycin, which will significantly reduce or eliminate the membrane potential, while retaining the ΔpH. By comparing the results of cytochrome bo_3 alone and cytochrome bo_3 with valinomycin in Figure 5, it is clear that valinomycin lowers the leaking rate (see also Figure S5). On average, the presence of valinomycin reduced the leaking rate by 60%, confirming that a significant membrane potential is present and thus that proton transfer by cytochrome bo_3 contributes to the formation of both terms of the PMF in our single-enzyme experiments (ΔpH and membrane potential). The relative frequency, however, with which cytochrome bo_3 enters the leak state is not reduced by the presence or absence of valinomycin. As without valinomycin, the relative frequency of entering the leak state is correlated to the ΔpH in the presence of valinomycin (Figure S6, see SI for a further discussion on the effect of valinomycin on the proton transport activity of cytochrome bo_3). These observations suggest that entering the leak state may be primarily triggered by the ΔpH, though we cannot fully exclude that a larger membrane potential can also trigger a leak state. In contrast, the rate of the proton back flow once a leak state is obtained seems to be driven by both elements of the PMF (Figure 5) suggesting that the leak state is due to a protein conformation that allows protons to freely flow backward, in a fashion similar to a proton channel.

■ CONCLUSION

We conclude that a long-lifetime leak state exists in cytochrome bo_3 during continuous enzyme turnover, which allows the back flow of protons. The leak state and the stalling in enzyme activity may act as a safety fuse that is triggered by excessive ΔpH during respiration in *E. coli*. Previous study shows that ROS production in mitochondria may be much more sensitive to ΔpH than to membrane potential.[41] Although seemingly inefficient in terms of energy conservation, proton leakage in small subpopulations of HCOs in a living organism might help to alleviate respiratory pressure and factors related to ROS production. The existence of the long-lifetime proton leak state and the stalling phase may provide an unprecedented insight into the proton pumping mechanism and its regulation in HCOs. Deciphering the precise role of proton leakage of proton transporters as well as its dependence on regulatory inputs and point mutations by assays like these will pave the way for controlling transport related diseased states.

■ MATERIALS AND METHODS

Protein Purification and Reconstitution. All chemicals were purchased from Sigma-Aldrich unless otherwise stated. Wild-type and E286C cytochrome bo_3 were purified from *Escherichia coli* C43 strains with the bo_3 gene knocked out from chromosome, where proteins were expressed from pET plasmids containing the corresponding gene sequences.[39] Wild-type cytochrome bo_3 was also purified from GO105/pJRhisA[42] for comparison. Proteins were purified similarly as previously reported.[35] Cytochrome bo_3 concentration was determined by its Soret band at 409 nm (ε = 188 mM^{-1} cm^{-1}). Protein was reconstituted following a method published previously,[17] except 20 mM MOPS buffer was used instead of HEPES. Before Bio-Beads were added, the pH sensitive dye, 8-hydroxypyrene-1,3,6-trisulfonic acid trisodium salt (HPTS), was added to a final concentration of 5 mM. The lipid mixture used for the reconstitution was *E. coli* polar lipid extract (Avanti Polar Lipids, Inc., Alabama, U.S.A.) mixed with the following: 1% (w/w) ubiquinone-10 and 0.4% (w/w) ATTO-633 labeled DOPE (ATTO-TEC GmbH, Germany). The protein-to-lipid weight percentage added for the reconstitution is 0.2%. Insoluble materials, possibly denatured protein, were removed by low-speed centrifugation at 17 000 RCF for 5 min at the end of the reconstitution. Standard BCA and Schaffner & Weissmann assays were both used to quantify the amount of protein that is actually reconstituted into lipid vesicles, and the loss of lipid during reconstitution was also quantified by the absorption of the ATTO633 labeled lipid. The results show that the final protein to dry lipid ratio (w/w) is 0.073 ± 0.004%. To estimate the average number of bo_3 complexes in a single vesicle, the following values were used: the protein/lipid weight ratio (0.073%), the size of the vesicle (70 nm), the thickness of the lipid bilayer (5 nm), the average surface area of the lipid headgroup (65 $Å^2$), the molecular weight of the protein (144 kDa), and the average molecular weight of the lipid (760). Under the assumption that a lipid vesicle is a double-layered sphere with an outer diameter of 70 nm and an inner diameter of 70 − 2 × 5 = 60 nm, one can calculate the number of lipid molecules in a vesicle. Using the protein/lipid ratio, one can further calculate, on average, how many protein complexes are present in a vesicle. Dynamic light scattering data showed that (proteo)liposomes in this study were highly monodispersed and are about 70 nm in diameter (Figure S7).

Electrochemistry-Microscopy Measurement. The experimental setup was refined from a method reported previously[42] to enable single-molecule measurements. Template-stripped gold electrodes with highly smooth transparent gold layers on glass substrates were functionalized with a 6-mercapto-1-hexanol (6-MH) self-assembled monolayer (SAM). They were prepared by the following procedure: 30-nanometer gold layers were thermally evaporated on polished silicon wafers (IDB Technologies Ltd., U.K.) with an Edwards Auto 306 evaporator (Edwards, U.K.) at a pressure $\leq 2 \times 10^{-6}$ millibar. Standard-thickness glass coverslips were then glued to the gold layer with a low-fluorescence epoxy glue (301−2FL, Epoxy Technology, Inc., Massachusetts, U.S.A.). After the glue cured, coverslips were carefully removed from the silicon wafers, during which the gold layer was stripped off the wafers, retaining the high smoothness of the silicon wafer template. The SAM layer was made by incubating the gold electrodes in 1 mM 6-MH solution in water overnight at 20 °C. The gold electrode is a part of a custom-built electrochemical cell that can be used with an inverted epi-fluorescence microscope (Eclipse Ti−U, Nikon Instruments, U.K.). After assembling the electrochemical cell, (proteo)liposomes were sparsely absorbed to the gold electrode by incubating the gold surface with a diluted suspension (2 μg/mL lipid) for 30 min at 20 °C followed by a thorough washing step to remove unbound (proteo)liposomes and nonencapsulated HPTS dye. We note that the experiments are conducted under ambient conditions and in ensemble experiments we have previously shown that this ensures that cytochrome bo_3 remains saturated with oxygen throughout the experiment.[36]

Images and image series were recorded using a 60× oil immersion objective (N.A. = 1.40, Nikon Instruments, U.K.), and an Andor Zyla 5.5 sCMOS Camera system (Andor Technology Ltd., U.K.). Fluorescence filters used in this study were from Chroma Technology Corporation (Vermont, U.S.A.): (1) D470/20X, excitation of one of the HPTS channels; (2) D410/30X, for excitation in another HPTS channel; (3) HQ535/48M, emission of both HPTS channels; (4) 500dcxr, dichroic mirror for both HPTS channels; (5) HQ620/60X, excitation of the ATTO633 fluorescence; (6) HQ700/75M, emission of the ATTO633 fluorescence; (7) Q660lp, dichroic mirror for ATTO633 fluorescence. The original images are 2560-by-2160 pixel/179-by-151 μm. The magnification is 60 (objective) × 1.5 (relay lens) = 90 times. The exposure time is 1 s for each channel, and the frame rate is 2.6 s^{-1}, including 0.6 s for rotating the filter cubes. A typical

DOI: 10.1021/jacs.5b08798
J. Am. Chem. Soc. 2015, 137, 16055−16063

image series contains about 500−1000 lipid vesicles. Examples of the full-scale images are shown in Figure S9.

A potentiostat (Chi604c, CH Instruments, Inc., Texas, U.S.A.) was used to control the potential between the working electrode (the gold electrode with lipid vesicles) and a Ag/AgCl/sat. KCl (199 mV vs Standard Hydrogen Electrode, SHE) reference electrode (Radiometer Analytical SAS, France). A platinum wire was used as the counter electrode. When the potential is applied to the gold electrode, the ubiquinone pool in the vesicles' lipid bilayer is electrochemically reduced and after diffusion through the vesicle, donates electrons to cytochrome bo_3, initiating oxygen reduction and proton uptake/release. Recording of image series was initiated while the potentiostat was switched off. After a given amount of time (typically 30 or 100 s) the potentiostat cell was switched on to maintain a constant potential of −0.2 V vs SHE for 100 s. This potential is optimal based on previous results.[42] The potentiostat was then switched off again but the image recording would continue for certain amount of time (typically 100 or 150 s). When the electrochemical potential is terminated, the proton uptake/release activity is found to halt within the time resolution of this study and, thus, the enzyme activity is tightly controlled by the potentiostat. There is a minimum of 15 min waiting period between each recording to allow the ΔpH and membrane potential to dissipate, and the fields of view of different recording sessions do not overlap. Typically 5 recordings were done on each gold electrode due to the limit of their available surface area. Each experimental system (wild-type bo_3, E286C mutant and valinomycin) contains data collected from different batches of preparation and each batch contains recordings from multiple electrodes. The numbers of independent lipid vesicles analyzed in each of the three experimental system described in the main text were on the scale of 19 000−30 000, of which about 3000 vesicles exhibit proton uptake/release.

Experiments with valinomycin added were done with the following steps. Cytochrome bo_3 was reconstituted using the same protocol as above and valinomycin was added to a final concentration of 10 μM with the lipid concentration adjusted to 4.4 mg/mL. The approximate molar ratio of valinomycin to lipid is 1.8×10^{-3}. The valinomycin was incubated with (proteo)liposomes for 15 min before further dilution to 2 μg/mL lipid and absorption onto the gold electrode, as above. However, after unbound (proteo)liposomes and nonencapsulated HPTS dye were removed by washing, a new valinomycin/liposome mixture (10 μM and 4.4 mg/mL, respectively; liposomes were without HPTS or cytochrome bo_3) was added to the solution to replenish the loss of valinomycin during the incubation and washing and keep the ratio of lipid and valinomycin relatively constant. Since the liposomes added here do not contain any fluorescent dye or fluorescently labeled lipid, they do not interfere with the image recording.

Data Analysis. Before the start of an experiment a single fluorescence image was taken to obtain the ATTO-633 fluorescence intensity of individual (proteo)liposomes containing 0.4% (w/w) ATTO-633 labeled DOPE. This image was used to calculate the diameter of the (proteo)liposomes with a method similar to that previously published.[43] Dynamic light scattering (Zetasizer Nano ZS, Malvern Instruments Ltd., U.K.) data were used to establish a calibration curve between ATTO-633 fluorescence and the diameter of the vesicles. Figure S8 shows that the conversion from ATTO fluorescence to diameter does not distort the size distribution of the lipid vesicles.

Fluorescent image time-traces were recorded alternating between the excitation filters for HPTS fluorescence. Image series were registered and corrected for drifting using ImageJ StackReg plug-in.[44] All subsequent analysis was performed in MATLAB R2012a (MathWorks, Massachusetts, U.S.A.) using user-written code. Lipid vesicles were identified on each frame of the image series and a two-dimensional Gaussian function was used to fit each vesicle HPTS fluorescence image. Using user-written code, comprehensive and automatic quality checking was carried out for each fitting on every frame to eliminate conglomerates, close-by vesicles, vesicle desorption during recording and vesicles on the edge of images. The code was written assuming the following: (1) single vesicles will appear as circular bright spots on the image; (2) because the bright spots are sparsely distributed on the images, the majority of them are single vesicles; (3) a cluster of vesicles will appear either noncircular or much larger. An automated image analysis was performed with MATLAB to remove noncircular spots or spots larger than expected for single vesicles. As the vesicles are sparsely adsorbed, an accurate value for the background intensity can be determined. Vesicles are then identified by the MATLAB code by finding pixels above certain threshold intensity. Then a 12-by-12 (pixel) local image (~0.84 × 0.84 μm) around the bright pixel was fitted to a 2-dimension Gaussian function. The fitting returns 4 parameters (baseline, amplitude, X-spread and Y-spread) and the fitting error at each pixel. These results are used to reject bright spots with the following characteristics: (1) fitting error above 20% (comparing to the original intensity data) at any pixel; (2) fitting error above 10% overall (in the 12-by-12 area); (3) circularity below 0.8; (4) fwhm is below 35 nm (= 0.5 pixel) or above 175 nm (= 2.5 pixel); (5) amplitude above background is below 1000 AU (arbitrary unit, background is about 3000 AU with a standard deviation about 150 AU); (6) baseline above 10 000 AU (this is usually concurrent with a large fwhm); (7) too close to the edge of image (6 pixel); (8) having another bright spot within 700 nm; (9) the fitted center is more than 2 pixel away from the brightest pixel (this is usually concurrent with a large fwhm); (10) in addition, after all images in a movie are fitted, if any of the above criteria is not satisfied in more than 30% of the frames of the movie, the vesicle is rejected entirely. The above criteria were chosen because they result in picking circular and separated bright spots with a typical size that is consistent with single vesicles.

The ratio of the fluorescence intensity of HPTS with the two excitation filters was used to calculate the pH inside the individual (proteo)liposome at the time of measurement. A calibration curve was established to convert the ratiometric HPTS data to pH. This calibration was done by measuring single (proteo)liposomes' HPTS fluorescence in the same procedure as described above at different pH values. Different pH points were achieved by changing the bulk solution's pH and adding 100 ng/mL nigericin and 100 ng/mL gramicidin to equilibrate the intravesicular pH with the outside. Because of the presence of gramicidin and nigericin, the intravesicular pH equals the pH of the bulk solution, and the bulk solution pH was measured. Therefore, the calibration procedure can effectively control the intravesicular pH. The fluorescence images for pH-fluorescence calibration were taken using the same procedure as the movies. The fluorescence data and pH were fitted to a Henderson−Hasselbalch equation and the parameters obtained were used to convert HPTS ratiometric fluorescence to intravesicular pH during turnover of cytochrome bo_3. The fitting results are given in Supporting Information (Figure S10 and Table S1). The number of protons taken/released was then calculated based on the diameter of lipid vesicle, the pH change and the buffering effect of MOPS buffer, HPTS and the lipids. We note that the obtained time traces, such as shown in Figure 2, are qualitatively identical irrespective of whether pH or cumulative number of transported protons is plotted (compare Figure 2 with Figure S1). To calculate the cumulative number of transported protons, the concentrations of MOPS buffer and HPTS encapsulated within the lipid vesicles were assumed to be the same as the bulk solution. The buffering capacity of lipids was determined empirically by a titration beforehand while the lipid surface area of single vesicles was calculated from the vesicle size. The buffering capacity of MOPS and HPTS are calculated using the Henderson−Hasselbalch equation. Each (proteo)liposome's change in the pH and the number of taken/released protons were then calculated and stored.

The sections of time traces recorded after the applied potential was switched off were fitted with an exponential decay function. The sections of the time traces within the potential window were then analyzed using user-written code to detect the proton taken up/released and leaking events. This automatic analysis is based on the hypothesis that a correlation between the pH/number-of proton taken up/released and time indicates either an active proton uptake/release or leaking event. It consists of fitting the data to models of one or multiple joint lines and, for each line (segment), the calculation of

DOI: 10.1021/jacs.5b08798
J. Am. Chem. Soc. 2015, 137, 16055−16063

Kendall tau rank correlation coefficient. In order to prevent overfitting of the trace by multiple lines, the fitting would start with a single linear regression (a single segment). If the standard deviation of the residual was less than 110% of the standard deviation of the trace, the procedure was stopped and the Kendall tau value determined. The standard deviation of the trace is independently determined using the data prior to the application of the potential. It is assumed that the intravesicular pH before the applying a potential is constant and that the noise level is consistent during the entire trace. If the standard deviation of the residual of the segment is higher than 110%, the data is fitted to two joined segments (i.e., the start of the second segment joins with the end of the first segment), where an iterative process is used to determine, based on the best fit, at which time-point the two segments are connected. If any of the segments still has a residue with a standard deviation above 110%, this process is continued.

To further check if the use of multiple segments is statistically justified, adjusted R^2 values are determined for fits using one, two or more segments, and the fit with the highest adjusted R^2 value is used. Adjusted R^2 takes into account the degrees of freedom in relation to the number of fitted parameters. *P*-values were calculated as part of the Kendall test on the resolved sections from the model fitting and only the sections of time traces with *P*-values below the threshold of 0.05 (95% confidence level) were accepted as proton uptake/release or leaking events. Proton uptake/release or leaking rates are taken from the slopes of the segments. The data was analyzed with higher and lower confidence levels and was found to be qualitatively identical. Finally, a leak event is defined as a change in the sign of a slope for two adjoining segments, where it is assumed that the first segment is due to active proton uptake/release.

■ ASSOCIATED CONTENT

Supporting Information

The Supporting Information is available free of charge on the ACS Publications website at DOI: 10.1021/jacs.5b08798.

Supporting figures and tables; Simulations to test the occurrence of two (proteo)liposomes closer than 200 nm apart; Errors and confidence levels, pH calibration procedure; Errors and confidence levels, fitting procedure; Activity of cytochrome bo_3 and the effect of valinomycin; Independent verification of experimental setup and data analysis; SI references. (PDF)

■ AUTHOR INFORMATION

Corresponding Authors

*stamou@nano.ku.dk
*hatzakis@nano.ku.dk
*l.j.c.jeuken@leeds.ac.uk

Notes

The authors declare no competing financial interest.

■ ACKNOWLEDGMENTS

The research leading to these results has received funding from the European Research Council under the European Union's Seventh Framework Programme (FP/2007-2013)/ERC Grant Agreement n. 280518 (M.L., R.P. and L. J.). D.S., N.H and S.J. acknowledge funding from the Lundbeck Foundation Center of Excellence Biomembranes in Nanomedicine, the SYNBIO Center for Synthetic Biology of the University of Copenhagen and N.S.H. acknowledges the Villum foundation "young investigator program". We thank Professor Robert Gennis from University of Illinois at Urbana−Champaign for providing the *E. coli* strains.

■ REFERENCES

(1) Pereira, M. M.; Santana, M.; Teixeira, M. *Biochim. Biophys. Acta, Bioenerg.* **2001**, *1505*, 185.
(2) Abramson, J.; Riistama, S.; Larsson, G.; Jasaitis, A.; Svensson-Ek, M.; Laakkonen, L.; Puustinen, A.; Iwata, S.; Wikstrom, M. *Nat. Struct. Biol.* **2000**, *7*, 910.
(3) Iwata, S.; Ostermeier, C.; Ludwig, B.; Michel, H. *Nature* **1995**, *376*, 660.
(4) Hirata, K.; Shinzawa-Itoh, K.; Yano, N.; Takemura, S.; Kato, K.; Hatanaka, M.; Muramoto, K.; Kawahara, T.; Tsukihara, T.; Yamashita, E.; Tono, K.; Ueno, G.; Hikima, T.; Murakami, H.; Inubushi, Y.; Yabashi, M.; Ishikawa, T.; Yamamoto, M.; Ogura, T.; Sugimoto, H.; Shen, J. R.; Yoshikawa, S.; Ago, H. *Nat. Methods* **2014**, *11*, 734.
(5) Blomberg, M. R. A.; Siegbahn, P. E. M. *Biochim. Biophys. Acta, Bioenerg.* **2014**, *1837*, 1165.
(6) Brzezinski, P.; Adelroth, P. *Curr. Opin. Struct. Biol.* **2006**, *16*, 465.
(7) Kaila, V. R. I.; Verkhovsky, M. I.; Wikstrom, M. *Chem. Rev.* **2010**, *110*, 7062.
(8) Rich, P. R.; Marechal, A. *J. R. Soc., Interface* **2013**, DOI: 10.1098/rsif.2013.0183.
(9) Yoshikawa, S.; Shimada, A. *Chem. Rev.* **2015**, *115*, 1936.
(10) Siletsky, S. A.; Konstantinov, A. A. *Biochim. Biophys. Acta, Bioenerg.* **2012**, *1817*, 476.
(11) Ogura, T. *Biochim. Biophys. Acta, Bioenerg.* **2012**, *1817*, 575.
(12) Kim, Y. C.; Hummer, G. *Biochim. Biophys. Acta, Bioenerg.* **2012**, *1817*, 526.
(13) Popovic, D. M.; Stuchebrukhov, A. A. *Biochim. Biophys. Acta, Bioenerg.* **2012**, *1817*, 506.
(14) Blomberg, M. R. A.; Siegbahn, P. E. M. *Biochim. Biophys. Acta, Bioenerg.* **2012**, *1817*, 495.
(15) Ferguson-Miller, S.; Hiser, C.; Liu, J. *Biochim. Biophys. Acta, Bioenerg.* **2012**, *1817*, 489.
(16) Kadenbach, B. *Biochim. Biophys. Acta, Bioenerg.* **2003**, *1604*, 77.
(17) Verkhovskaya, M. L.; GarciaHorsman, A.; Puustinen, A.; Rigaud, J. L.; Morgan, J. E.; Verkhovsky, M. I.; Wikstrom, M. *Proc. Natl. Acad. Sci. U. S. A.* **1997**, *94*, 10128.
(18) Nelson, N.; Sacher, A.; Nelson, H. *Nat. Rev. Mol. Cell Biol.* **2002**, *3*, 876.
(19) Mills, D. A.; Tan, Z.; Ferguson-Miller, S.; Hosler, J. *Biochemistry* **2003**, *42*, 7410.
(20) Azizan, E. A. B.; Poulsen, H.; Tuluc, P.; Zhou, J.; Clausen, M. V.; Lieb, A.; Maniero, C.; Garg, S.; Bochukova, E. G.; Zhao, W.; Shaikh, L. H.; Brighton, C. A.; Teo, A. E. D.; Davenport, A. P.; Dekkers, T.; Tops, B.; Kuusters, B.; Ceral, J.; Yeo, G. S. H.; Neogi, S. G.; McFarlane, I.; Rosenfeld, N.; Marass, F.; Hadfield, J.; Margas, W.; Chaggar, K.; Solar, M.; Deinum, J.; Dolphin, A. C.; Farooqi, I. S.; Striessnig, J.; Nissen, P.; Brown, M. J. *Nat. Genet.* **2013**, *45*, 1055.
(21) Kaneko, M.; Desai, B. S.; Cook, B. *Nat. Genet.* **2014**, *46*, 144.
(22) Murphy, M. P. *Biochem. J.* **2009**, *417*, 1.
(23) Finkel, T.; Holbrook, N. J. *Nature* **2000**, *408*, 239.
(24) Droge, W. *Physiol. Rev.* **2002**, *82*, 47.
(25) Belevich, I.; Verkhovsky, M. I.; Wikstrom, M. *Nature* **2006**, *440*, 829.
(26) Faxen, K.; Gilderson, G.; Adelroth, P.; Brzezinski, P. *Nature* **2005**, *437*, 286.
(27) von Ballmoos, C.; Gennis, R. B.; Adelroth, P.; Brzezinski, P. *Proc. Natl. Acad. Sci. U. S. A.* **2011**, *108*, 11057.
(28) Kaila, V. R. I.; Verkhovsky, M. I.; Hummer, G.; Wikstrom, M. *Proc. Natl. Acad. Sci. U. S. A.* **2008**, *105*, 6255.
(29) Min, W.; English, B. P.; Luo, G. B.; Cherayil, B. J.; Kou, S. C.; Xie, X. S. *Acc. Chem. Res.* **2005**, *38*, 923.
(30) Hatzakis, N. S.; Wei, L.; Jorgensen, S. K.; Kunding, A. H.; Bolinger, P. Y.; Ehrlich, N.; Makarov, I.; Skjot, M.; Svendsen, A.; Hedegard, P.; Stamou, D. *J. Am. Chem. Soc.* **2012**, *134*, 9296.
(31) Zhao, Y. F.; Terry, D. S.; Shi, L.; Quick, M.; Weinstein, H.; Blanchard, S. C.; Javitch, J. A. *Nature* **2011**, *474*, 109.
(32) Busch, K.; Tampe, R. *Rev. Mol. Biotechnol.* **2001**, *82*, 3.

DOI: 10.1021/jacs.5b08798
J. Am. Chem. Soc. 2015, 137, 16055−16063

(33) Mathiasen, S.; Christensen, S. M.; Fung, J. J.; Rasmussen, S. G.; Fay, J. F.; Jorgensen, S. K.; Veshaguri, S.; Farrens, D. L.; Kiskowski, M.; Kobilka, B.; Stamou, D. *Nat. Methods* **2014**, *11*, 931.
(34) Larsen, J.; Hatzakis, N. S.; Stamou, D. *J. Am. Chem. Soc.* **2011**, *133*, 10685.
(35) Rumbley, J. N.; Nickels, E. F.; Gennis, R. B. *Biochim. Biophys. Acta, Protein Struct. Mol. Enzymol.* **1997**, *1340*, 131.
(36) Weiss, S. A.; Bushby, R. J.; Evans, S. D.; Jeuken, L. J. C. *Biochim. Biophys. Acta, Bioenerg.* **2010**, *1797*, 1917.
(37) Kuyper, C. L.; Kuo, J. S.; Mutch, S. A.; Chiu, D. T. *J. Am. Chem. Soc.* **2006**, *128*, 3233.
(38) Gurtovenko, A. A.; Vattulainen, I. *J. Am. Chem. Soc.* **2005**, *127*, 17570.
(39) Egawa, T.; Ganesan, K.; Lin, M. T.; Yu, M. A.; Hosler, J. P.; Yeh, S. R.; Rousseau, D. L.; Gennis, R. B. *Biochim. Biophys. Acta, Bioenerg.* **2011**, *1807*, 1342.
(40) Oshea, P. S.; Azzi, A. *Biochem. J.* **1984**, *224*, 343.
(41) Lambert, A. J.; Brand, M. D. *Biochem. J.* **2004**, *382*, 511.
(42) Daskalakis, N. N.; Muller, A.; Evans, S. D.; Jeuken, L. J. C. *Soft Matter* **2011**, *7*, 49.
(43) Kunding, A. H.; Mortensen, M. W.; Christensen, S. M.; Stamou, D. *Biophys. J.* **2008**, *95*, 1176.
(44) Thevenaz, P.; Ruttimann, U. E.; Unser, M. *IEEE T. Image Process.* **1998**, *7*, 27.

DOI: 10.1021/jacs.5b08798
J. Am. Chem. Soc. 2015, 137, 16055−16063